AGU ADVANCING EARTH AND SPACE SCIENCE

Geophysical Research Letters

RESEARCH LETTER
10.1029/2021GL093339

Key Points:

- Indo-Pacific precipitation isotopes are dominated by glacial-interglacial climate shifts for 560 ky
- Precipitation isotope records from eastern China are dominated by the 23 and 19 ky precessional cycles for 640 ky
- Indo-Pacific climate is linked to high latitude processes, cautioning against assuming local insolation dominates

Supporting Information:

Supporting Information may be found in the online version of this article.

Correspondence to:

G. Windler,
gwindler@email.arizona.edu

Citation:

Windler, G., Tierney, J. E., & Anchukaitis, K. J. (2021). Glacial-interglacial shifts dominate tropical Indo-Pacific hydroclimate during the late Pleistocene. *Geophysical Research Letters*, *48*, e2021GL093339. https://doi.org/10.1029/2021GL093339

Received 10 MAR 2021
Accepted 12 JUL 2021

Glacial-Interglacial Shifts Dominate Tropical Indo-Pacific Hydroclimate During the Late Pleistocene

Grace Windler[1], Jessica E. Tierney[1], and Kevin J. Anchukaitis[1,2,3]

[1]Department of Geosciences, University of Arizona, Tucson, AZ, USA, [2]School of Geography, Development, and Environment, University of Arizona, Tucson, AZ, USA, [3]Laboratory of Tree-Ring Research, University of Arizona, Tucson, AZ, USA

Abstract The climatic drivers of tropical rainfall and atmospheric circulation in the late Pleistocene are still debated. Some studies suggest that tropical precipitation primarily responded to precession (23–19 ky cycle), whereas others propose that glacial-interglacial (100 ky) changes in ice sheets and sea level dominate. Here, we reexamine orbital influences on tropical-to-subtropical precipitation isotopes using singular spectrum analysis to isolate leading oscillatory modes from proxy records across the Indo-Pacific Warm Pool (IPWP) and Asian monsoon domain. We find that the IPWP, Bay of Bengal, and South China Sea are dominated by the 100 ky glacial-interglacial mode of variability, whereas eastern China clearly follows precession, suggesting that precipitation isotopes over the mid-latitude Asian continent respond to different mechanisms than those in the IPWP or Indian and East Asian monsoon regions. This study demonstrates that glacial cycles, rather than changes in local insolation, are the dominant drivers of Pleistocene IPWP hydroclimate.

Plain Language Summary Reconstructions of past changes in rainfall, derived from cave deposits and ancient leaf waxes, provide an opportunity to understand how the tropical Indo-Pacific Warm Pool, located between Southeast Asia and Australia, responds to large-scale changes in global climate. Here, we statistically analyze five long records of rainfall and atmospheric circulation across the Warm Pool, the Indian and East Asian monsoon regions, and eastern China to isolate different external drivers of change between regions for the last 600,000 years. We find that the signal over eastern China is dominated by seasonal changes in solar radiation over mid-latitudes in the Northern Hemisphere, whereas the signal in the Warm Pool and monsoon regions are dominated by changes in sea level and high latitude ice sheet growth. This clear spatial difference in the external drivers of regional circulation changes suggests that the cave records from China do not exclusively reflect East Asian monsoon rainfall. Additionally, this study supports a strong connection between high and low latitude climates during the last several hundred thousand years.

1. Introduction

The Indo-Pacific Warm Pool (IPWP) has the warmest sea surface temperatures (SSTs) in the tropics and some of the highest annual precipitation on the planet. The IPWP sits under the ascending branch of two Walker Circulation cells, where converging surface winds and warm SSTs supply large amounts of water vapor to the atmosphere. Today, rainfall gradients in the IPWP follow the seasonal position of the Intertropical Convergence Zone (ITCZ), which is in the Northern Hemisphere (NH) during boreal summer and shifts to the Southern Hemisphere during boreal winter (Aldrian & Dwi Susanto, 2003; Schott et al., 2009). Accordingly, some studies suggest that tropical precipitation changes on geological timescales primarily respond to the 23- and 19-ky precession cycles in Earth's orbit (Clement et al., 2004; Jalihal et al., 2019; Merlis et al., 2013), which control the seasonal amount of incoming solar radiation (insolation). The precession theory posits that when NH summer insolation is high, average ITCZ position is farther north, resulting in wetter conditions over northern IPWP and eastern China. Precessional signals in atmospheric methane reconstructions from ice cores have been used to support this theory, that is, high NH insolation leads to increased monsoon intensity and tropical methane production (Guo et al., 2012; Ruddiman & Raymo, 2003), although the tropical control on these records has recently come into question (Thirumalai et al., 2020). Alternatively, other studies suggest that IPWP precipitation is more sensitive to changes in ice sheets and sea level over glacial-interglacial time scales, where exposure of the Sunda and Sahul Shelves altered moisture

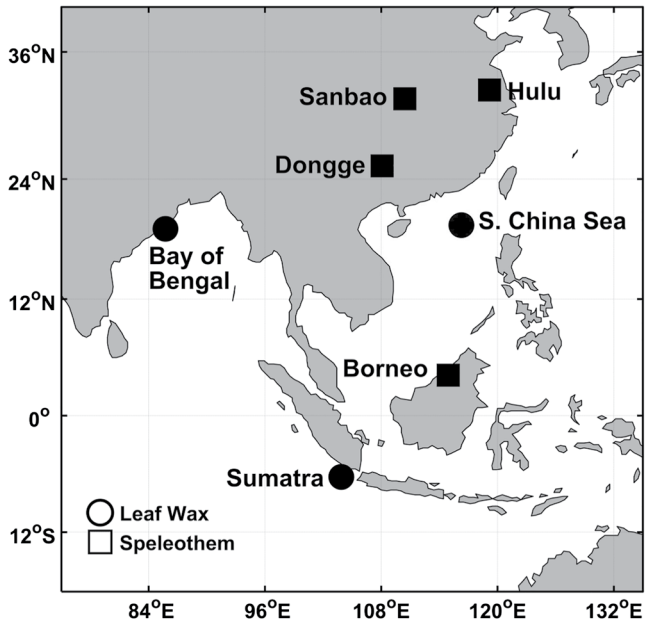

Figure 1. Locations discussed in this text.

fluxes and pathways (DiNezio et al., 2018; Griffiths et al., 2009). Glacial cycles have a 100 ky pacing over the late Pleistocene, related to the rhythmic timing of high latitude ice-volume growth and termination (Lisiecki & Raymo, 2005).

Speleothem $\delta^{18}O(\delta^{18}O_{speleo})$ and leaf wax $\delta D(\delta D_{wax})$ from sediment cores are powerful hydrologic tracers and are commonly used to reconstruct hydroclimate in the IPWP (Ayliffe et al., 2013; Niedermeyer et al., 2014), the Indian- (Kathayat et al., 2016; McGrath et al., 2021), and the East Asian-monsoon regions (Liu et al., 2014; Wang et al., 2001). Precipitation isotopes vary with moisture transport, rainfall, and convective processes (Conroy et al., 2013; Kurita, 2013; Midhun et al., 2018; Moore et al., 2014), thus complicating interpretations of $\delta^{18}O_{speleo}$ and δD_{wax}. For instance, $\delta^{18}O_{speleo}$ in eastern China show strong precessional variability and are thought to indicate changes in East Asian summer monsoon (EAM) intensity in accordance with NH insolation (Cheng et al., 2016; Liu et al., 2014; Wang et al., 2001); however, this remains highly debated since other regional proxies conflict with the cave spectral signature and suggest that the EAM is more sensitive to 100 ky variability in high latitude ice sheets and greenhouse gases (Beck et al., 2018; Clemens et al., 2010, 2018; Sun et al., 2015).

Similarly, Borneo $\delta^{18}O_{speleo}$—the longest precipitation isotope record in the IPWP—has been used to argue that precessional changes in NH insolation are the primary influence on IPWP precipitation for the last ~560 ky (Carolin et al., 2016); however, other proxy records from the IPWP suggest otherwise. Southern IPWP leaf wax $\delta^{13}C$ data indicate that drier conditions varied in connection with NH ice volume, rather than insolation (Russell et al., 2014; Windler et al., 2019) and leaf wax-derived precipitation $\delta D\left(\delta D_{precip}\right)$ from southern Sumatra suggests that glacial-interglacial cycles dominate IPWP circulation for the last 450 ky (Windler et al., 2020). SSTs from the IPWP have also been found to vary with glacial cycles since ~500 ka (Lea, 2004; Windler et al., 2019).

Here, we reexamine orbital influences on IPWP precipitation isotopes and their connection to sub-tropical monsoon regions to the north using singular spectrum analysis (SSA) of five long proxy records (Figure 1). These records are of sufficient length and resolution to reveal the major orbital frequencies, including the 100 ky glacial-interglacial cycle, 41 ky obliquity cycle, and 23- and 19-ky precession cycles. SSA is a well-established nonparametric technique used to decompose time series into trends and oscillations that collectively contribute to variability in the original data (Allen & Smith, 1997; Ghil & Vautard, 1991; Vautard et al., 1992). SSA provides an empirical filter for examining variability and is useful for paleoclimate reconstructions as it allows isolation of signals within noisy time series (Ghil et al., 2002). Here, we use SSA to filter the proxy data, identify, and interpret leading modes of variability, and examine their frequency spectra to evaluate the relative contribution of orbital influences.

2. Materials and Methods

2.1. Paleoclimate Data

Southern Sumatra δD_{precip} is derived from leaf waxes extracted from MD98-2152 (6.33°S, 103.88°E) (Windler et al., 2020) and spans 450–0 ka with an average resolution of ~2,500 years (Figure 2a). Due to the missing interval from 42 to 30 ka (Figure 2a), we focus our SSA on the continuous part of the record before 42 ka. The Bay of Bengal record is from the International Ocean Discovery Program Site U1446 (19.08°N, 85.73°E) (McGrath et al., 2021). This record covers 640–0 ka with an average resolution of ~2,000 years (Figure 2d). The δD_{precip} values were calculated from δD_{wax} using leaf wax $\delta^{13}C$ values in the same core to account for vegetation shifts over time, following the methodology of Windler et al. (2020).

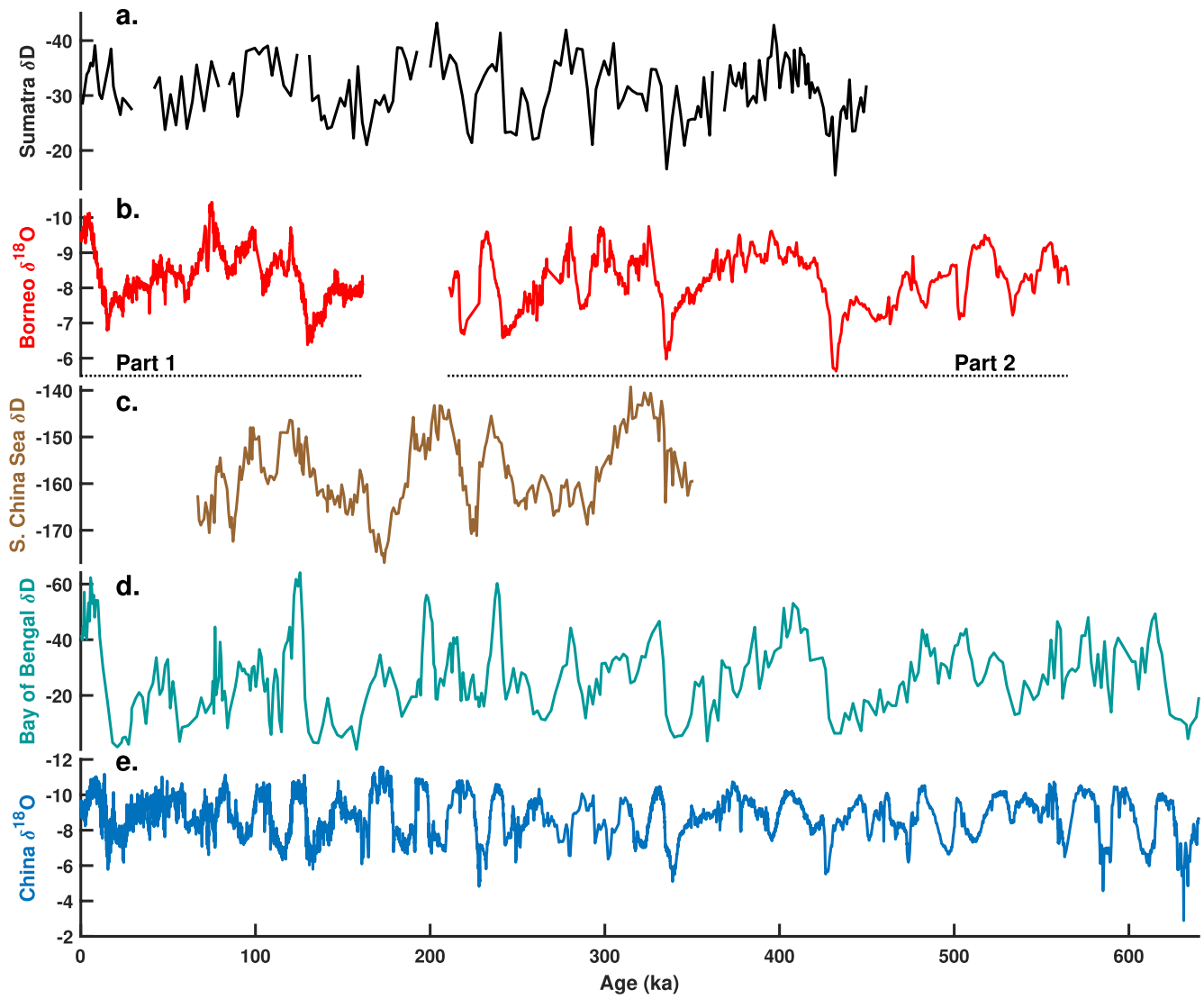

Figure 2. Paleoclimate data used in this study. (a) Sumatra δD_{precip} (Windler et al., 2020). (b) Borneo1 $\delta^{18}O_{speleo}$ (Carolin et al., 2016) and Borneo2 (Meckler et al., 2012). (c) South China Sea δD_{wax} (Thomas et al., 2014). (d) Bay of Bengal δD_{precip} (McGrath et al., 2021). (e) Composite China $\delta^{18}O_{speleo}$ (Cheng et al., 2016). All *y*-axes are reversed except panel (c).

Borneo (4.17°N, 114.91°E) $\delta^{18}O_{speleo}$ has a substantial interval of missing time (211–162 ka), so we analyze the data before and after this hiatus separately. The youngest portion (hereafter Borneo1) extends from 162 to 0 ka with an average resolution of 100 years (Carolin et al., 2016) and the older portion (hereafter Borneo2) covers 565–211 ka (Figure 2b). Borneo2 consists of compiled data from stalagmites analyzed in Meckler et al. (2012) with an average resolution of ~460 years.

South China Sea δD_{wax} is from Ocean Drilling Project Site 1146 (19.45°N, 116.27°E) (Thomas et al., 2014). This record spans 350–67 ka with an average resolution of ~1,100 years (Figure 2c). No leaf wax $\delta^{13}C$ data is available for this core, so we run our analysis on the raw δD_{wax} values. The composite $\delta^{18}O_{speleo}$ from China consists of data from Hulu (32.5°N, 119.17°E), Sanbao (31.67°N, 110.43°E, and Dongge (25.28°N, 108.08°E Caves (Figure 1). This record extends to 640 ka with an average resolution of ~77 years (Figure 2e) (Cheng et al., 2016). All $\delta D\left(\delta^{18}O_{speleo}\right)$ values are reported in ‰ notation versus Vienna Standard Mean Ocean Water (Vienna Pee Dee Belemnite).

SSA is performed on data with a consistent time step (Ghil et al., 2002), so we resample each record prior to analysis. Cave records (Borneo1, Borneo2, and China) are resampled to an even time step of 1,000 years. The marine records are lower in resolution and resampled as follows: Sumatra and the Bay of Bengal to 2,500 years and South China Sea to 1,500 years. The resampled time series retain the structure of the original data and are high enough in resolution to detect Earth's orbital cycles (Figure S1).

2.2. Singular Spectrum Analysis

We use SSA to isolate leading oscillatory modes of variability in each record (Allen & Smith, 1996, 1997; Ghil et al., 2002). SSA is performed by constructing a "trajectory matrix" consisting of M lagged copies of a centered and evenly sampled time series, then calculating the empirical orthogonal functions (EOFs) from the covariance matrix of the lagged series (Ghil et al., 2002; Ghil & Vautard, 1991; Vautard et al., 1992). Here, we use an embedded dimension (window width) M that is approximately equivalent to 1/5 the length of each resampled proxy record to construct the trajectory matrix (Ghil et al., 2002), then calculate the singular value decomposition of the $M \times M$ covariance matrix of the centered, evenly spaced data. We use the eigenvalues from the singular value decomposition to quantify the percent of variance explained by each eigenvector to identify the leading modes of variability in each time series. We then calculate the "reconstructed components" (RCs) by projecting the time series onto each mode following Ghil et al. (2002):

$$R_{\mathcal{K}}(t) = \frac{1}{M_t} \sum_{k \in \mathcal{K}} \sum_{j=L_t}^{U_t} A_k(t - j + 1)\rho_k(j) \quad (1)$$

where the reconstruction is based on a set of modes $(\mathcal{K})$, M_t is the embedded dimension, U_t and L_t are the upper and lower bounds of summation, A_k refers to the principal components, and ρ_k are the eigenvectors of the lagged covariance matrix. Combining RCs of the meaningful modes in the data emphasizes major patterns of variability that comprise the proxy record (Figure S2).

To assess how many leading modes might reflect actual physical processes in the Earth system (Monahan et al., 2009), we perform a series of nonparametric statistical tests using both heuristic and Monte Carlo red- and white-noise simulations (Allen & Smith, 1996, 1997; Jackson, 1993; Overland & Preisendorfer, 1982; Preisendorfer & Mobley, 1988). When generating red noise, we estimate the first order autoregressive correlation, AR(1), from each record. Each centered random series is then analyzed as described above to calculate null eigenvalues and their associated eigenvectors. We repeat this process 10,000 times for each location and test. To identify interpretable modes of variability from each SSA, we determine which combination of leading modes explains the majority of the variance in each record and estimate the dominant frequency of these modes using a smoothed periodogram (Bloomfield, 2004). We calculate the raw periodogram of the linearly detrended RC of each mode individually and smooth the spectra with a six-point Gaussian filter.

Although nonparametric statistical tests can suggest which modes exceed variability expected from some noise model, this does not guarantee that they reflect distinct deterministic processes in the Earth system (Monahan et al., 2009). Additionally, the missing time interval in Borneo limits the length of the data to two individual segments of 161 and 354 ky (Figure 2b) and makes assessing the significance of individual peaks near 100 ky highly sensitive to both window width M and the AR(1) coefficient. To determine whether the leading modes are indeed physically meaningful, we compare the combined RCs with independent time series known to record changes in Earth's orbital parameters or climate state: δ^{18}O from benthic foraminifera (Lisiecki & Raymo, 2005) and the astronomical precession solution (Laskar et al., 2004).

3. Results

The leading six modes of Sumatra, four modes of Borneo1, six modes of Borneo2, six modes of South China Sea, nine modes (excluding mode 7) of the Bay of Bengal, and eight modes of the composite from China potentially reflect physical climatic processes. Each SSA has some modes that are in quadrature (having similar, but out-of-phase EOFs and the same frequency (Ghil et al., 2002)), so we combine these paired RCs for analysis (Figure 3). Spectral power and explained variance for the interpretable modes of variability are presented in Figure 3.

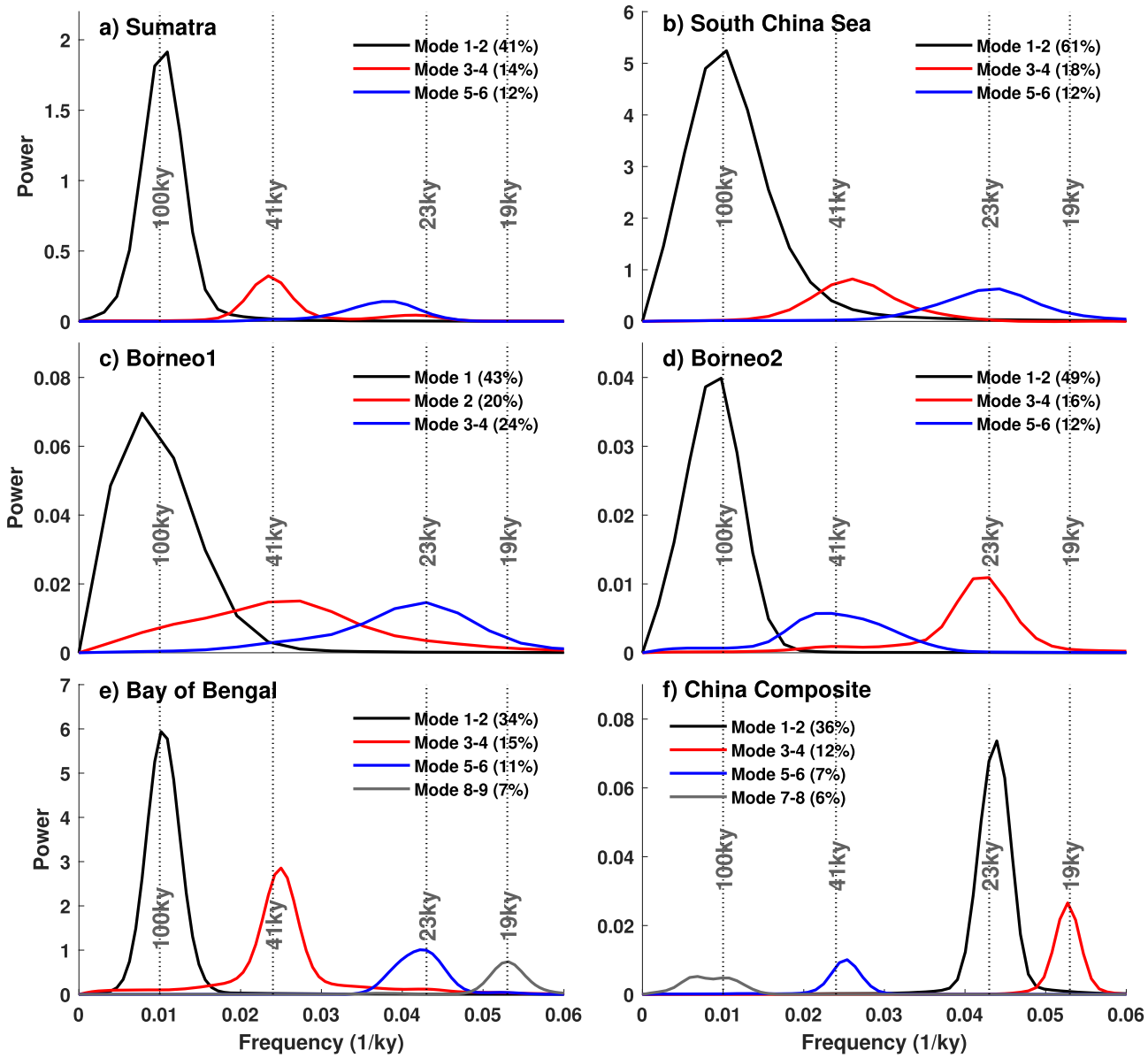

Figure 3. Smoothed periodograms of leading modes for (a) Sumatra, (b) South China Sea, (c and d) Borneo, (e) Bay of Bengal, and (f) China. Modes that are in quadrature are listed as pairs. Explained variance for each mode are listed in each panel.

For all locations except China, the leading mode (or pair) that explains the largest percentage of variance in the data shows peak spectral power corresponding to the 100 ky glacial-interglacial mode of variability (Figure 3). The leading mode in China $\delta^{18}O_{speleo}$ peaks at frequencies corresponding to the 23 ky precession cycle (Figure 3f). Modes explaining the second-most variance differ by location. Modes 3 & 4 of Borneo1 and Borneo2 (24% and 16% of the variance, respectively) peak at frequencies corresponding to the 23 ky precessional cycle (Figures 3c and 3d). Similarly, modes 5 & 6 and 8 & 9 of the Bay of Bengal (18% of the total variance) correspond to the 23- and 19-ky precessional cycles, respectively (Figure 3e). Modes 3 & 4 explain 12% of the variance in China and peak at 19 ky precessional frequency (Figure 3f). In contrast, modes 3 & 4 in both Sumatra and South China Sea show peak spectral power at the 41 ky obliquity cycle (Figures 3a and 3b).

RCs of interpretable modes of variability for each location are shown in Figure 4. Leading RCs for Sumatra, Borneo, South China Sea, and the Bay of Bengal generally align with the benthic $\delta^{18}O$ stack (Figures 4a–4d),

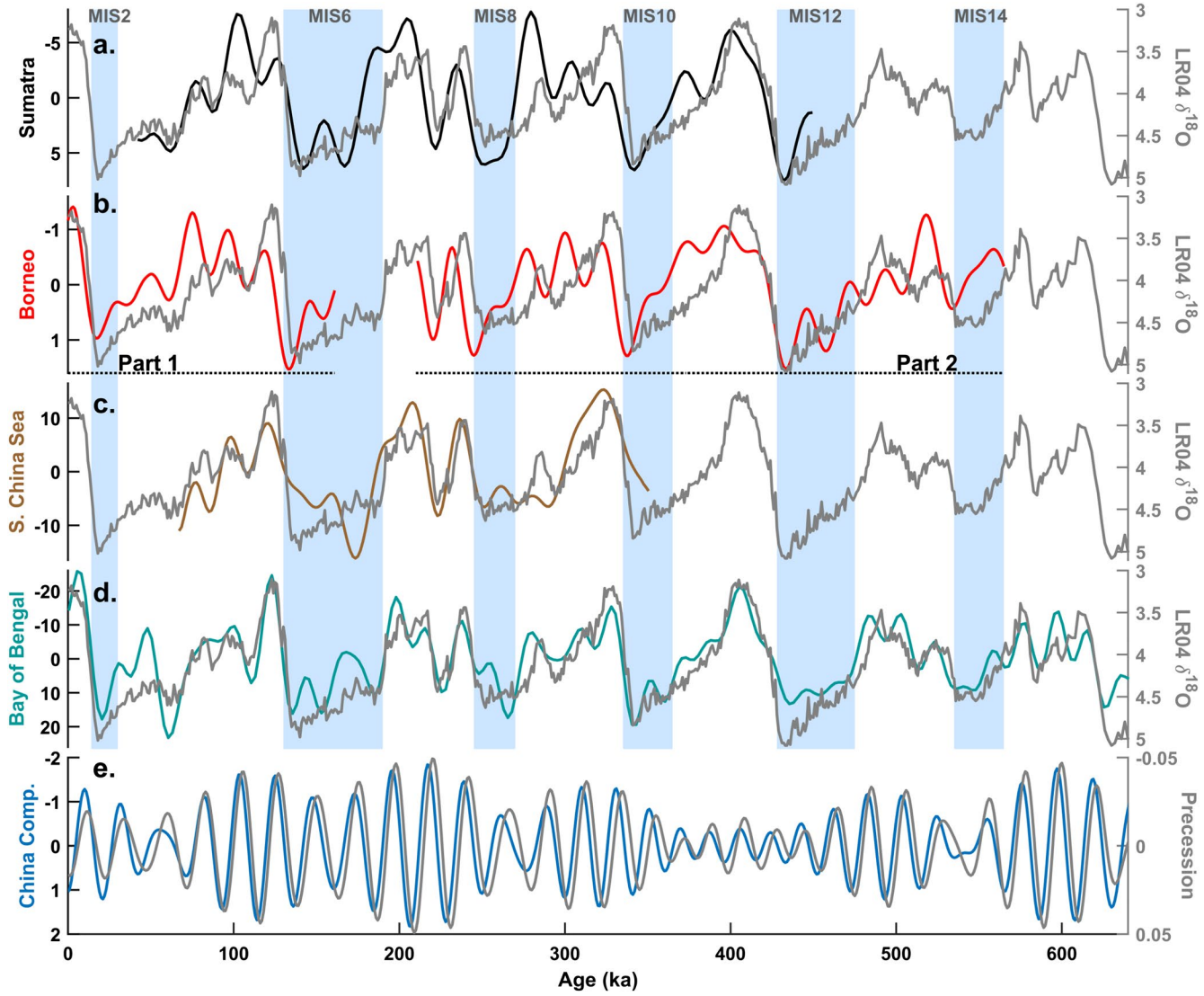

Figure 4. Reconstructed components (RCs) of meaningful modes of variability for (a) Sumatra: modes 1–6, (b) Borneo: modes 1–4 from Borneo1 and modes 1–6 from Borneo2, (c) South China Sea: modes 1–6, (d) Bay of Bengal: modes 1–9 excluding mode 7, and (e) China: modes 1–4. RCs are plotted against either the LR04 benthic stack (Lisiecki & Raymo, 2005) (panels a–d), or precession (Laskar et al., 2004) (panel c). All *y*-axes are reversed except panel (c) Glacial marine isotope stages are highlighted in blue.

which reflects deep ocean temperature and global ice volume (Lisiecki & Raymo, 2005). Specifically, RCs from Sumatra, Borneo, and the Bay of Bengal have maxima that correspond with the timing of glacial marine isotope stages (MIS) 2, 6, 8, 10, 12, and 14 (Figures 4a, 4b and 4d), whereas RCs from the South China Sea have minima during glacial MIS 6, 8, and 10 (Figure 4c). Leading RCs for China $\delta^{18}O_{speleo}$ track precession closely throughout the record (Figure 4e). Additionally, many of the minima in Sumatra, Borneo, and the Bay of Bengal, or maxima in South China Sea RCs occur roughly concurrently with either interglacial periods or minimal precession values (Figure 4).

4. Discussion

The 100 ky glacial-interglacial cycle is the dominant mode of variability in Borneo and Sumatra, the two IPWP locations (Figure 3). This finding contrasts with previous, largely qualitative, claims that Borneo $\delta^{18}O_{speleo}$ is insensitive to glacial-interglacial climate changes and instead dominated by insolation over

precessional timescales (Carolin et al., 2013, 2016; Partin et al., 2007). A potential cause of the greater 100 ky sensitivity at Borneo in our analysis is the absence of an ice volume-correction. During glacial periods, the global deep ocean is isotopically enriched due to increased global ice volume (Duplessy et al., 2002) and precipitation isotope reconstructions are commonly corrected to attempt to account for this offset; however, doing so assumes that surface waters from which meteoric water is sourced experience the same net change as the deep ocean. In reality, surface waters may vary from the deep ocean offset, so assuming a homogeneous correction potentially obscures local and regional processes recorded in the isotope proxies (Windler et al., 2020). To preserve spatial differences between locations, we did not correct for global ice volume. To explore whether this affected our results, we performed an identical analysis on ice volume-corrected Borneo $\delta^{18}O_{speleo}$. The ice volume-correction does reduce the variance associated with the 100 ky cycle and increase that of the precessional cycle; however, glacial-interglacial variability remains the dominant component of the record (Figure S3).

Age model uncertainties may affect the timing of variability in proxy records, potentially obscuring different orbital signals in the data. This is unlikely to be an issue in Borneo1, which has a tightly constrained chronology (~±400 years average 2σ) (Carolin et al., 2013, 2016). Likewise, age uncertainties in Sumatra and China are low enough (each averaging under ±2 ky 2σ) to be reasonably certain that precession, obliquity, and glacial-interglacial changes can be resolved (Cheng et al., 2016; Windler et al., 2019). Age uncertainties for the Bay of Bengal and South China Sea, while not explicitly quantified, are likely to be similar to Sumatra, since they are also marine cores dated with tie points. Borneo2 age uncertainties are larger between 550 and 320 ka (~±10 ky average 2σ) due to open-system exchange at one of the sites (Meckler et al., 2012). These age errors are large enough to potentially compromise the precessional resolution in Borneo2; however, this is not observed in our SSA results (i.e., Borneo2 and Borneo1 show comparable results, Figure 3).

The importance of glacial-interglacial variability at Borneo, Sumatra, and the South China Sea is consistent with the hypothesis that sea level changes are the primary drivers of IPWP hydroclimate during the late Pleistocene. Global changes in ice volume have a large impact on the sea level, affecting the land-sea distribution over the Maritime Continent: during glacial periods the sea level was lower than today (Waelbroeck et al., 2002) and the Sunda and Sahul Shelves were exposed. Proxy-model comparisons have demonstrated that sea level and NH ice sheet albedo exert a first order control on rainfall (DiNezio et al., 2018; DiNezio & Tierney, 2013) and precipitation isotopes (Windler et al., 2020) in the IPWP during the Last Glacial Maximum (LGM). Specifically, it resulted in a decoupling of the Indian and Pacific Walker Circulation cells during the LGM leading to widespread drying across the exposed area and a spatially distinct precipitation isotope response with increased low-level moisture convergence (divergence) causing a lighter (heavier) isotope signal over the Pacific (Indian) Ocean side of the IPWP (Windler et al., 2020). Notably, the South China Sea δD_{wax} becomes isotopically lighter during glacial periods (Figure 4c), which is consistent with the simulated precipitation isotope response to sea level and ice sheet albedo in Windler et al. (2020). Similarly, the secondary precession modes appear to influence the South China Sea and Sumatra/Bay of Bengal in opposite ways (Figure 4), following regional patterns of seasonal precipitation changes driven by insolation reported in Tierney et al. (2012). The SSA results here confirm that glaciation, as opposed to changes in seasonal insolation, is the dominant process influencing circulation over the IPWP during the late Pleistocene.

In contrast to other locations, China $\delta^{18}O_{speleo}$ is overwhelmingly dominated by precession (Figure 3f). The spatial coherency and strong influence of precession in the Chinese caves is well known; however, the mechanisms governing $\delta^{18}O_{speleo}$ changes preserved there remain contested. Initially interpreted to reflect EAM strength (Cheng et al., 2016; Wang et al., 2001), subsequent studies have countered this idea, variously suggesting that winter temperatures, as well as precipitation isotopes in the winter and fall seasons, impact the $\delta^{18}O_{speleo}$ over China (Clemens et al., 2010), or that the records reflect upstream distillation from either the Indian monsoon (Battisti et al., 2014; Pausata et al., 2011), or the EAM (Liu et al., 2014) systems. Dominant moisture sources of the EAM are the tropical eastern Indian and western Pacific Oceans and, following NH insolation, higher land-sea temperature contrasts result in monsoon enhancement and isotopically lighter precipitation over eastern China (Liu et al., 2014). Our SSA results counter this theory. If China $\delta^{18}O_{speleo}$ represented EAM intensity, with water sourced from the tropical Indian and Pacific Oceans, then the spectral composition of eastern Chinese cave records would more closely resemble the IPWP and South China Sea. NH ice sheets may have restricted the northern extent of the ITCZ and EAM (Lu et al., 2013).

If this mechanism imprinted on regional precipitation isotopes, then the spectral composition of China $\delta^{18}O_{speleo}$ would more closely resemble the IPWP. Our SSA shows that they are spectrally distinct (Figure 3).

A recent study similarly showed that $\delta^{18}O_{speleo}$ records from eastern China are spectrally distinct from precipitation isotope records in the Indian monsoon domain, including the Bay of Bengal record used here (McGrath et al., 2021). Our SSA results confirm the dominance of 100 ky variability in the Bay of Bengal as presented by McGrath et al. (2021), who conclude that the Indian monsoon and EAM are decoupled during the late Pleistocene. The distinct spectral configurations between these regions (Figures 3e and 3f) contradicts the theory that eastern China $\delta^{18}O_{speleo}$ reflects upstream moisture sources from the Indian monsoon region (Pausata et al., 2011; Battisti et al., 2014). In addition to ice volume, McGrath et al. (2021) find that Bay of Bengal δD_{precip} is in phase with greenhouse gas concentration maxima during the late Pleistocene; however, isotope-enabled simulations have shown that greenhouse gas forcing is expected to cause lighter precipitation isotope values across the entire IPWP and Bay of Bengal during glacial periods, whereas ice sheets/sea level result in the glacial enrichment visible in the Bay of Bengal, Borneo, and Sumatra (Windler et al., 2020).

Our SSA highlights that the Chinese cave isotopic signal is unique in the context of data from not only the Indian monsoon region (McGrath et al., 2021), but also the IPWP and South China Sea, which are dominated by 100 ky cycles (Figure 3). While a full diagnosis of the dynamics behind the nearly "pure" precessional signature of China $\delta^{18}O_{speleo}$ is outside the scope of this paper, we hypothesize that it must be related to a mid-latitude mechanism; otherwise, we would expect its tempo to more closely match that of tropical moisture from the IPWP and Indian monsoon regions. Chiang et al. (2015) posited that China $\delta^{18}O_{speleo}$ reflects the seasonal position of the mid-latitude jet, which varies with insolation: when summer insolation is lower (higher) the jet is located farther south (north), and its position limits (allows) the transport of isotopically light tropical moisture over the Asian continental interior, leading to isotopically heavier (lighter) rainfall over China (Chiang et al., 2015). This mechanism explains the precessional beat of eastern China $\delta^{18}O_{speleo}$, the abrupt transitions seen in the cave data as the jet position passes north or south of the Tibetan Plateau, and why China behaves so differently than the isotopic records from the Bay of Bengal, South China Sea, and IPWP.

Regardless of the precise mechanism causing precessional scale variability in China $\delta^{18}O_{speleo}$, many interpretations of these data assume that there is an implicit connection with deep tropical processes, such as remote moisture sources in the eastern Indian and western Pacific Oceans. While precessional signals are identified in the precipitation isotope records from these regions, they are secondary modes of variability. The different frequencies of the dominant modes between eastern China and the other locations (Figure 3) highlights that IPWP and Indian monsoon circulation are primarily driven by different mechanisms than $\delta^{18}O_{speleo}$ from China. Our SSA results indicate a strong connection between deep tropical IPWP circulation and high latitude processes, while seasonal insolation is a secondary control. Conversely, the strong precessional power in China $\delta^{18}O_{speleo}$ suggests that seasonal insolation exerts a powerful influence on mid-latitude dynamics.

5. Conclusions

We have identified the major orbital forcing mechanisms influencing precipitation isotope records from southern Sumatra, northern Borneo, South China Sea, the Bay of Bengal, and eastern China over the late Pleistocene. We used SSA as an empirical filter to isolate leading modes of variability in each reconstruction and the orbital frequencies with which these modes vary. The 100 ky glacial-interglacial mode is dominant at every location except the caves in eastern China, where precessional cycles overwhelmingly dominate. Our SSA results contrast with previous reports that Borneo $\delta^{18}O_{speleo}$ is insensitive to glacial-interglacial climate changes and emphasize that mid-latitude processes over the Asian continent are not strongly coupled to circulation over the IPWP and Indian monsoon region through time. Furthermore, this study highlights the strong connections between high- and low-latitude processes and cautions against assuming that insolation dominates tropical circulation during the late Pleistocene.

Data Availability Statement

The data used in this study have been previously published and are available as follows: Borneo1 $\delta^{18}O$ through Carolin et al. (2016), Borneo2 $\delta^{18}O$ through Meckler et al. (2012), Sumatra δD through Windler et al. (2020), Bay of Bengal δD through (McGrath et al., 2021), South China Sea δD through (Thomas et al., 2014), and the China composite $\delta^{18}O$ through Cheng et al. (2016).

Acknowledgments
Funding for this study was provided by the David and Lucile Packard Foundation Fellowship in Science and Engineering to J.E. Tierney and by the National Science Foundation Graduate Research Fellowship Program to G. Windler (grant DGE-1746060).

References

Aldrian, E., & Dwi Susanto, R. (2003). Identification of three dominant rainfall regions within Indonesia and their relationship to sea surface temperature. *International Journal of Climatology: A Journal of the Royal Meteorological Society*, *23*(12), 1435–1452. https://doi.org/10.1002/joc.950

Allen, M. R., & Smith, L. A. (1996). Monte Carlo SSA: Detecting irregular oscillations in the presence of colored noise. *Journal of Climate*, *9*(12), 3373–3404. https://doi.org/10.1175/1520-0442(1996)009<3373:mcsdio>2.0.co;2

Allen, M. R., & Smith, L. A. (1997). Optimal filtering in singular spectrum analysis. *Physics Letters A*, *234*(6), 419–428. https://doi.org/10.1016/s0375-9601(97)00559-8

Ayliffe, L. K., Gagan, M. K., Zhao, J.-X., Drysdale, R. N., Hellstrom, J. C., Hantoro, W. S., et al. (2013). Rapid interhemispheric climate links via the Australasian monsoon during the last deglaciation. *Nature Communications*, *4*(1), 1–6. https://doi.org/10.1038/ncomms3908

Battisti, D., Ding, Q., & Roe, G. (2014). Coherent pan-Asian climatic and isotopic response to orbital forcing of tropical insolation. *Journal of Geophysical Research: Atmospheres*, *119*(21), 11–997. https://doi.org/10.1002/2014jd021960

Beck, J. W., Zhou, W., Li, C., Wu, Z., White, L., Xian, F., et al. (2018). A 550,000-year record of East Asian monsoon rainfall from ^{10}Be in loess. *Science*, *360*(6391), 877–881. https://doi.org/10.1126/science.aam5825

Bloomfield, P. (2004). *Fourier analysis of time series: An introduction*. John Wiley & Sons.

Carolin, S. A., Cobb, K. M., Adkins, J. F., Clark, B., Conroy, J. L., Lejau, S., et al. (2013). Varied response of western pacific hydrology to climate forcings over the last glacial period. *Science*, *340*(6140), 1564–1566. https://doi.org/10.1126/science.1233797

Carolin, S. A., Cobb, K. M., Lynch-Stieglitz, J., Moerman, J. W., Partin, J. W., Lejau, S., et al. (2016). Northern Borneo stalagmite records reveal West Pacific hydroclimate across MIS 5 and 6. *Earth and Planetary Science Letters*, *439*, 182–193. https://doi.org/10.1016/j.epsl.2016.01.028

Cheng, H., Edwards, R. L., Sinha, A., Spötl, C., Yi, L., Chen, S., et al. (2016). The Asian monsoon over the past 640,000 years and ice age terminations. *Nature*, *534*(7609), 640–646. https://doi.org/10.1038/nature18591

Chiang, J. C., Fung, I. Y., Wu, C.-H., Cai, Y., Edman, J. P., Liu, Y., et al. (2015). Role of seasonal transitions and westerly jets in East Asian paleoclimate. *Quaternary Science Reviews*, *108*, 111–129. https://doi.org/10.1016/j.quascirev.2014.11.009

Clemens, S. C., Holbourn, A., Kubota, Y., Lee, K., Liu, Z., Chen, G., & Fox-Kemper, B. (2018). Precession-band variance missing from East Asian monsoon runoff. *Nature Communications*, *9*(1), 1–12. https://doi.org/10.1038/s41467-018-05814-0

Clemens, S. C., Prell, W. L., & Sun, Y. (2010). Orbital-scale timing and mechanisms driving late Pleistocene Indo-Asian summer monsoons: Reinterpreting cave speleothem $\delta^{18}O$. *Paleoceanography*, *25*(4). https://doi.org/10.1029/2010pa001926

Clement, A. C., Hall, A., & Broccoli, A. (2004). The importance of precessional signals in the tropical climate. *Climate Dynamics*, *22*(4), 327–341. https://doi.org/10.1007/s00382-003-0375-8

Conroy, J. L., Cobb, K. M., & Noone, D. (2013). Comparison of precipitation isotope variability across the tropical Pacific in observations and SWING2 model simulations. *Journal of Geophysical Research: Atmospheres*, *118*(11), 5867–5892. https://doi.org/10.1002/jgrd.50412

DiNezio, P. N., & Tierney, J. E. (2013). The effect of sea level on glacial Indo-Pacific climate. *Nature Geoscience*, *6*(6), 485–491. https://doi.org/10.1038/ngeo1823

DiNezio, P. N., Tierney, J. E., Otto-Bliesner, B. L., Timmermann, A., Bhattacharya, T., Rosenbloom, N., & Brady, E. (2018). Glacial changes in tropical climate amplified by the Indian Ocean. *Science advances*, *4*(12), eaat9658. https://doi.org/10.1126/sciadv.aat9658

Duplessy, J.-C., Labeyrie, L., & Waelbroeck, C. (2002). Constraints on the ocean oxygen isotopic enrichment between the last glacial maximum and the Holocene: Paleoceanographic implications. *Quaternary Science Reviews*, *21*(1–3), 315–330. https://doi.org/10.1016/s0277-3791(01)00107-x

Ghil, M., Allen, M., Dettinger, M., Ide, K., Kondrashov, D., Mann, M., et al. (2002). Advanced spectral methods for climatic time series. *Reviews of Geophysics*, *40*(1), 3–1. https://doi.org/10.1029/2000rg000092

Ghil, M., & Vautard, R. (1991). Interdecadal oscillations and the warming trend in global temperature time series. *Nature*, *350*(6316), 324–327. https://doi.org/10.1038/350324a0

Griffiths, M. L., Drysdale, R. N., Gagan, M., Zhao, J.-X., Ayliffe, L., Hellstrom, J. C., et al. (2009). Increasing Australian–Indonesian monsoon rainfall linked to early Holocene sea-level rise. *Nature Geoscience*, *2*(9), 636–639. https://doi.org/10.1038/ngeo605

Guo, Z., Zhou, X., & Wu, H. (2012). Glacial-interglacial water cycle, global monsoon and atmospheric methane changes. *Climate Dynamics*, *39*(5), 1073–1092. https://doi.org/10.1007/s00382-011-1147-5

Jackson, D. A. (1993). Stopping rules in principal components analysis: A comparison of heuristical and statistical approaches. *Ecology*, *74*(8), 2204–2214. https://doi.org/10.2307/1939574

Jalihal, C., Bosmans, J. H. C., Srinivasan, J., & Chakraborty, A. (2019). The response of tropical precipitation to earth's precession: The role of energy fluxes and vertical stability. *Climate of the Past*, *15*(2), 449–462. https://doi.org/10.5194/cp-15-449-2019

Kathayat, G., Cheng, H., Sinha, A., Spötl, C., Edwards, R. L., Zhang, H., et al. (2016). Indian monsoon variability on millennial-orbital timescales. *Scientific Reports*, *6*(1), 1–7. https://doi.org/10.1038/srep24374

Kurita, N. (2013). Water isotopic variability in response to mesoscale convective system over the tropical ocean. *Journal of Geophysical Research: Atmospheres*, *118*(18), 10–376. https://doi.org/10.1002/jgrd.50754

Laskar, J., Robutel, P., Joutel, F., Gastineau, M., Correia, A., & Levrard, B. (2004). A long-term numerical solution for the insolation quantities of the earth. *Astronomy & Astrophysics*, *428*(1), 261–285. https://doi.org/10.1051/0004-6361:20041335

Lea, D. W. (2004). The 100 000-yr cycle in tropical SST, greenhouse forcing, and climate sensitivity. *Journal of Climate*, *17*(11), 2170–2179. https://doi.org/10.1175/1520-0442(2004)017<2170:tycits>2.0.co;2

Lisiecki, L. E., & Raymo, M. E. (2005). A Pliocene-Pleistocene stack of 57 globally distributed benthic $\delta^{18}O$ records. *Paleoceanography*, *20*(1), PA1003. https://doi.org/10.1029/2004pa001071

Liu, Z., Wen, X., Brady, E., Otto-Bliesner, B., Yu, G., Lu, H., et al. (2014). Chinese cave records and the East Asia summer monsoon. *Quaternary Science Reviews*, *83*, 115–128. https://doi.org/10.1016/j.quascirev.2013.10.021

Lu, H., Yi, S., Liu, Z., Mason, J. A., Jiang, D., Cheng, J., et al. (2013). Variation of East Asian monsoon precipitation during the past 21 ky and potential CO_2 forcing. *Geology*, *41*(9), 1023–1026. https://doi.org/10.1130/g34488.1

McGrath, S. M., Clemens, S. C., Huang, Y., & Yamamoto, M. (2021). Greenhouse gas and ice volume drive Pleistocene Indian summer monsoon precipitation isotope variability. *Geophysical Research Letters*, *48*(4), e2020GL092249. https://doi.org/10.1029/2020gl092249

Meckler, A., Clarkson, M., Cobb, K., Sodemann, H., & Adkins, J. (2012). Interglacial hydroclimate in the tropical west Pacific through the late Pleistocene. *Science*, *336*(6086), 1301–1304. https://doi.org/10.1126/science.1218340

Merlis, T. M., Schneider, T., Bordoni, S., & Eisenman, I. (2013). The tropical precipitation response to orbital precession. *Journal of Climate*, *26*(6), 2010–2021. https://doi.org/10.1175/jcli-d-12-00186.1

Midhun, M., Lekshmy, P., Ramesh, R., Yoshimura, K., Sandeep, K., Kumar, S., et al. (2018). The effect of monsoon circulation on the stable isotopic composition of rainfall. *Journal of Geophysical Research: Atmospheres*, *123*(10), 5205–5221. https://doi.org/10.1029/2017jd027427

Monahan, A. H., Fyfe, J. C., Ambaum, M. H., Stephenson, D. B., & North, G. R. (2009). Empirical orthogonal functions: The medium is the message. *Journal of Climate*, *22*(24), 6501–6514. https://doi.org/10.1175/2009jcli3062.1

Moore, M., Kuang, Z., & Blossey, P. (2014). A moisture budget perspective of the amount effect. *Geophysical Research Letters*, *41*(4), 1329–1335. https://doi.org/10.1002/2013gl058302

Niedermeyer, E. M., Sessions, A. L., Feakins, S. J., & Mohtadi, M. (2014). Hydroclimate of the western indo-pacific warm pool during the past 24,000 years. *Proceedings of the National Academy of Sciences*, *111*(26), 9402–9406. https://doi.org/10.1073/pnas.1323585111

Overland, J. E., & Preisendorfer, R. (1982). A significance test for principal components applied to a cyclone climatology. *Monthly Weather Review*, *110*(1), 1–4. https://doi.org/10.1175/1520-0493(1982)110<0001:astfpc>2.0.co;2

Partin, J. W., Cobb, K. M., Adkins, J. F., Clark, B., & Fernandez, D. P. (2007). Millennial-scale trends in west Pacific warm pool hydrology since the last glacial maximum. *Nature*, *449*(7161), 452–455. https://doi.org/10.1038/nature06164

Pausata, F. S., Battisti, D. S., Nisancioglu, K. H., & Bitz, C. M. (2011). Chinese stalagmite $\delta^{18}O$ controlled by changes in the Indian monsoon during a simulated Heinrich event. *Nature Geoscience*, *4*(7), 474–480. https://doi.org/10.1038/ngeo1169

Preisendorfer, R. W., & Mobley, C. D. (1988). Principal component analysis in meteorology and oceanography. *Developments in Atmospheric Science*, *17*.

Ruddiman, W. F., & Raymo, M. E. (2003). A methane-based time scale for Vostok ice. *Quaternary Science Reviews*, *22*(2–4), 141–155. https://doi.org/10.1016/s0277-3791(02)00082-3

Russell, J. M., Vogel, H., Konecky, B. L., Bijaksana, S., Huang, Y., Melles, M., et al. (2014). Glacial forcing of central Indonesian hydroclimate since 60,000 y bp. *Proceedings of the National Academy of Sciences*, *111*(14), 5100–5105. https://doi.org/10.1073/pnas.1402373111

Schott, F. A., Xie, S.-P., & McCreary, J. P., Jr. (2009). Indian Ocean circulation and climate variability. *Reviews of Geophysics*, *47*(1), RG1002. https://doi.org/10.1029/2007rg000245

Sun, Y., Kutzbach, J., An, Z., Clemens, S., Liu, Z., Liu, W., et al. (2015). Astronomical and glacial forcing of East Asian summer monsoon variability. *Quaternary Science Reviews*, *115*, 132–142. https://doi.org/10.1016/j.quascirev.2015.03.009

Thirumalai, K., Clemens, S. C., & Partin, J. W. (2020). Methane, monsoons, and modulation of millennial-scale climate. *Geophysical Research Letters*, *47*(9), e2020GL087613. https://doi.org/10.1029/2020gl087613

Thomas, E. K., Clemens, S. C., Prell, W. L., Herbert, T. D., Huang, Y., Liu, Z., et al. (2014). Temperature and leaf wax 2h records demonstrate seasonal and regional controls on Asian monsoon proxies. *Geology*, *42*(12), 1075–1078. https://doi.org/10.1130/g36289.1

Tierney, J. E., Oppo, D. W., LeGrande, A. N., Huang, Y., Rosenthal, Y., & Linsley, B. (2012). The influence of Indian Ocean atmospheric circulation on warm pool hydroclimate during the Holocene epoch. *Journal of Geophysical Research: Atmospheres*, *117*(D19), D19108. https://doi.org/10.1029/2012jd018060

Vautard, R., Yiou, P., & Ghil, M. (1992). Singular-spectrum analysis: A toolkit for short, noisy chaotic signals. *Physica D: Nonlinear Phenomena*, *58*(1–4), 95–126. https://doi.org/10.1016/0167-2789(92)90103-t

Waelbroeck, C., Labeyrie, L., Michel, E., Duplessy, J. C., McManus, J., Lambeck, K., & Labracherie, M. (2002). Sea-level and deep water temperature changes derived from benthic foraminifera isotopic records. *Quaternary Science Reviews*, *21*(1–3), 295–305. https://doi.org/10.1016/s0277-3791(01)00101-9

Wang, Y.-J., Cheng, H., Edwards, R. L., An, Z., Wu, J., Shen, C.-C., & Dorale, J. A. (2001). A high-resolution absolute-dated late Pleistocene monsoon record from Hulu Cave, China. *Science*, *294*(5550), 2345–2348. https://doi.org/10.1126/science.1064618

Windler, G., Tierney, J. E., DiNezio, P. N., Gibson, K., & Thunell, R. (2019). Shelf exposure influence on Indo-Pacific Warm Pool climate for the last 450,000 years. *Earth and Planetary Science Letters*, *516*, 66–76. https://doi.org/10.1016/j.epsl.2019.03.038

Windler, G., Tierney, J. E., Zhu, J., & Poulsen, C. J. (2020). Unravelling glacial hydroclimate in the indo-pacific warm pool: Perspectives from water isotopes. *Paleoceanography and Paleoclimatology*, *35*, e2020PA003985. https://doi.org/10.1029/2020PA003985